

## REDUCTION OF CROSSTALK IN BLENDED-SHOT MIGRATION

*J. Schleicher, J. C. Costa, and A. Novais*

**email:** *js@ime.unicamp.br,jesse.ufpa@gmail.com,amelia@ime.unicamp.br*

**keywords:** *Wave-equation migration, shot blending, signal enhancement, multi-fold data, encoding*

### ABSTRACT

*When migrating more than one shot at the same time, the nonlinearity of the imaging condition causes the final image to contain the so-called crosstalk, i.e., the results of the interference of wavefields associated with different sources. In this work, we study various ideas of using weights in the imaging condition, called encoding, for the reduction of crosstalk. We combine the ideas of random phase and/or amplitude encoding and random alteration of the sign with additional multiplication with powers of the imaginary unit. This procedure moves part of the crosstalk to the imaginary part of the resulting image, leaving the desired crosscorrelation in the real part. In this way, the final image is less impaired. Our results indicate that with a combination of these weights, the crosstalk can be reduced by a factor of 4. Moreover, we evaluate the selection procedure of sources contributing to each group of shots. We compare random choice with a deterministic procedure, where the random numbers are exchanged for numbers similar to those of a Costas array. These numbers preserve certain properties of a random choice, but avoid the occurrence of patterns in the distribution. The objective is to avoid that nearby sources can be added to the same group of shots, which cannot be guaranteed with a random choice. Finally, we show that the crosstalk noise can be reduced after migration by image processing.*

### INTRODUCTION

Because of the great effort needed to migrate data from an acquisition consisting of a large number of sources, as required in 3D seismics, blended-shot migration processes data from more than one source simultaneously (Temme, 1984). This idea is based on the observation that the (full or one-way) wave equation is a linear operation, i.e., the wavefield produced by a set of sources is equal to the sum of the wavefields produced by each source acting alone.

The problem with this procedure arises when applying the image condition, conventionally a cross-correlation (Claerbout, 1971) between the wavefield propagated down from source and the recorded field, backpropagated from the receivers. When migrating shot groups, we replace the individual fields associated with a single source by a sum over a shot group. The result is a modified imaging consisting of two contributions, one being the desired image and other the interference from fields associated with different sources, called crosstalk. Thus, this procedure is only feasible in practice, if the crosstalk is considerably smaller than the desired image. Since the number of individual crosstalk contributions is higher than that those to the image, measures must be taken to reduce each of them in comparison to the desired image.

Several ideas on how to achieve the reduction of crosstalk have been discussed in the literature, based on the encoding of the sources, i.e., the inclusion of weights in the imaging condition. Ideally, we would like to choose the weights such that the resulting crosstalk matrix equals the unit matrix (Godwin and Sava, 2013, see also references there). This would mean no crosstalk. As this cannot be satisfied exactly, we need the best possible approximation.

One of the first proposals of shot encoding was plane-wave migration (Temme, 1984). The work of Romero et al. (2000) contains several proposals for phase encoding (linear, random, by frequency modulation – chirp). However, the noise reduction achieved in that study was not sufficient to allow for the sum of large numbers of sources. Other ideas include the alteration of the sign (Sun et al., 2002), source modulation (Soubaras, 2006), phase encoding using gold codes (Guerra and Biondi, 2008), random amplitude encoding (Godwin and Sava, 2010) and source decimation (Godwin and Sava, 2011). Godwin and Sava (2013) provide a comparison of several ideas of encoding.

In this work we combine the ideas of random phase and amplitude encoding and sign alteration with additional multiplication with the weight  $w_{gk} = \tilde{w}_{gk} = i^g$ . In this way, half the crosstalk passes to the imaginary part of the resulting image, while the desired image is unchanged. Thus, the real part of the modified image is less affected by crosstalk.

Additionally to encoding, we evaluate the influence of the choice of sources contributing to each shot group. We compare the random choice with a procedure, where the random numbers are exchanged for numbers similar to those of a Costas array (Costas, 1965; Golomb and Taylor, 1984; Drakakis and Rickard, 2010). These numbers preserve certain properties of a random choice, but avoid the occurrence of patterns in the distribution. The goal is to avoid coherent energy in the crosstalk by making sure that nearby sources cannot be added to the same shot group, which cannot be guaranteed with a random choice.

Finally, under the hypothesis that the crosstalk behaves like random noise with zero mean, we apply a denoising technique borrowed from image processing to the results of a blended-shot migration.

### BLEND-ED-SHOT MIGRATION

Wave-equation migration consists of two basic parts. The first part is the downward propagation of the source and receiver wavefields into the subsurface domain to be imaged. The second part is the application of an imaging condition to distinguish potential reflection points from points with no reflectivity under the current seismic survey.

The propagation part consists of the numerical solution of the (full or one-way) wave equation. Since the wave equation is a linear operation, the wavefield produced by a set of sources is equal to the sum of the wavefields produced by each source acting alone. Mathematically, we can write

$$\mathcal{L} \sum_{k=1}^N U_k = \sum_{k=1}^N \mathcal{L} U_k, \quad (1)$$

where  $\mathcal{L}$  denotes the wave-equation operator under consideration,  $U_k$  denotes the wavefield to be propagated, associated with source number  $k$ , and  $N$  is the number of simultaneously described wavefields.

Thus, the wave-propagation part of wave-equation migration can be carried out with several wavefields at once. Unfortunately, the same is not true for the imaging condition. Each individual image is constructed by crosscorrelation between the wavefield propagated down from source ( $D_k$ ) and the recorded field, back-propagated from the receivers ( $U_k$ ), at the same level in depth. The final image is then determined by the sum of the individual images of all common-shot gathers, i.e., the final image at each point  $\mathbf{x}$  is obtained as

$$I(\mathbf{x}) = \sum_{k=1}^N U_k \otimes D_k, \quad (2)$$

where the operator  $\otimes$  denotes the crosscorrelation.

As we can see from equation (2), the imaging condition is nonlinear. If we want to migrate  $K$  shot groups, we need to replace in equation (2) the individual fields associated with single sources by a sum over a shot group. Thus, we obtain

$$\tilde{I}(\mathbf{x}) = \sum_{g=1}^G \left( \sum_{k=1}^K U_k \right)_g \otimes \left( \sum_{j=1}^K D_j \right)_g = I + C, \quad (3)$$

where the sum over  $g$  represents the sum over groups and the other two sums are those over the shots constituting the groups. Therefore, the result is a modified image  $\tilde{I}$  consisting of two contributions, one

being the desired image  $I$  and other the interference from fields associated with different sources, called crosstalk. The latter is given by

$$C = \sum_{k=1}^N \sum_{j \neq k} U_k \otimes D_j . \quad (4)$$

Thus, this procedure is only feasible in practice, if it is possible to ensure that the contribution of crosstalk  $C$  is negligible in comparison to the contribution of the desired image  $I$ . Since the number of individual contributions to  $C$  is higher than that for  $I$ ,  $C$  can be greater than  $I$ , thus degrading the resulting image up to a point where it becomes useless. Therefore, measures must be taken to reduce  $C$  in comparison to the desired image  $I$ .

Several ideas on how to achieve the reduction of  $C$  have been discussed in the literature, based on the encoding of the sources, i.e., the inclusion of weights in equation (3) as

$$\tilde{I}(\mathbf{x}) = \sum_{g=1}^G \left( \sum_{k=1}^N w_{gk} U_k \right)_g \otimes \left( \sum_{j=1}^N \tilde{w}_{gj} D_j \right)_g = \hat{I} + C , \quad (5)$$

where  $\hat{I}$  is the image, modified by weights  $w_{gk}$  and  $\tilde{w}_{gk}$ . For each  $g$ , the weight vectors have  $K$  nonzero values for  $k$  between 1 and  $N$ . The weighting by these factors causes the final energy distribution between  $\hat{I}$  and  $C$  to depend on the crosstalk matrix

$$W_{kj} = \sum_{g=1}^G w_{gk} \tilde{w}_{gj}^* . \quad (6)$$

We observe that if the diagonal of matrix  $\mathbf{W}$  in equation (6) is composed only of unitary values, then the weighted image,  $\hat{I}$ , equals the desired image,  $I$ . Moreover, if the off-diagonal elements of this matrix are all zero, then no crosstalk remains in the final image. Thus, we recognize that ideally, we would like to choose the weights  $w_{gk}$  and  $\tilde{w}_{gj}$  such that

$$W_{kj} = \delta_{kj} , \quad (7)$$

with  $\delta_{kj}$  denoting the Kronecker delta. In this case, we would obtain  $C = 0$ , i.e., no crosstalk, and  $\tilde{I} = I$ . As equation (7) can not be satisfied exactly, we need the best possible approximation.

In this work we combine the ideas of random phase and amplitude encoding and sign alteration with additional multiplication with the weight  $w_{gk} = \tilde{w}_{gk} = i^g$ . In this way, half the crosstalk  $C$  passes to the imaginary part of the resulting image, while the desired image  $I$  is unchanged. Thus, the real part of the modified image (5) is less affected by crosstalk.

### Weight functions

All random encoding schemes make use of a random variable to calculate the weights. Let  $r_j$  denote the  $j$ -th realization of a random variable, uniformly distributed between 0 and 1. Using this notation, we can represent the weight functions under investigation as follows.

- Random phase encoding (between  $-\pi$  and  $\pi$ )

$$w_{gj} = \begin{cases} \exp\{i\pi(2r_j - 1)\} & \text{continuous} \\ \exp\{i\pi \frac{2[M r_j] - M + 1}{M - 1}\} & \text{discrete, } M \text{ levels} \end{cases} \quad (8)$$

and  $\tilde{w}_{gj} = w_{gj}$ .

- Random amplitude encoding (between  $-1$  and  $1$ )

$$w_{gj} = \begin{cases} 2r_j - 1 & \text{continuous} \\ (2[M r_j] - M + 1)/(M - 1) & \text{discrete, } M \text{ levels.} \end{cases} \quad (9)$$

Here, we also used  $\tilde{w}_{gj} = w_{gj}$ , although this choice degrades the quality of image  $\hat{I}$ . The choice  $\tilde{w}_{gj} = 1/w_{gj}$  would avoid this degradation, but introduces instabilities when the weights are very small.

- Random choice of sign (only factors  $-1$  or  $1$ )

$$w_{gj} = \text{sgn}(2r_j - 1) \quad \text{and} \quad \tilde{w}_{gj} = w_{gj} . \quad (10)$$

Note that this choice is a subset of both preceding ones. It corresponds to a two-level phase or amplitude encoding (phase  $-\pi$  and  $\pi$ , or amplitude  $-1$  e  $1$ ).

- Deterministic imaginary-unit weight per group

$$w_{gj} = i^g \quad \text{and} \quad \tilde{w}_{gj} = w_{gj} . \quad (11)$$

- Combinations of these weights, like the product of weights (8) and (9), (8) and (11), (10) and (11), (8), (9) and (11), etc.

In the above formulas, the operator  $[.]$  denotes the Gauss brackets, defining the largest integer less than its argument.

To evaluate the reduction in crosstalk in the migrated image achieved by these weights, we compare the matrices  $\mathbf{W}$  generated by the product (6) of the weights. An important number in this sense is the energy ratio between the off-diagonal and diagonal of matrix  $\mathbf{W}$ . The lower this number, the better  $\mathbf{W}$  approximates the desired relationship (7).

### Group composition

Another question regarding the grouping of shots for the purpose of migration refers to the selection of shots joined into groups. Besides classical choices like the simulation of plane or cylindrical waves, the random choice of shots is suggested in the literature. A possible problem with this approach is that by not controlling the choice, patterns can form that may affect the final image. An example for such patterns would be the choice of neighboring shots showing strong correlations between them. In this paper, we investigate a way to mitigate this problem through a technique that selects numbers minimizing the occurrence of patterns (“pattern-free”).

The technique is inspired by so-called Costas arrays (Costas, 1965; Golomb and Taylor, 1984; Drakakis and Rickard, 2010). A Costas array is a permutation of the unit matrix so that within the vector formed by all columns, there is no equal distance between two nonzero elements. Thus, a shift creates, at most, a coincidence of two such elements. These arrays are used to reduce crosstalk in radar and sonar systems (Beard et al., 2004).

Unfortunately, the construction of Costas arrays presents practical difficulties. First, Costas arrays of the dimensions 32 and 33 are not known in the literature. In addition, the definition of a Costas array as a permutation matrix with no special restrictions leads to a simple method to find them, because the Costas condition is not easily stated in a clear and simple set of restrictions. The only known way to find all Costas arrays for a given order is an exhaustive search. However, to check the Costas condition for all  $N!$  permutations of an array of order  $N$  is prohibitively expensive. Moreover, for large  $N$ , the chance to actually find a Costas array decreases, because the number of Costas arrays of order  $N$  drops quickly after reaching a maximum of 21,104 for  $N = 16$ . Beard et al. (2004) show that there are only 200 Costas arrays of order 24.

For these reasons, we opted for a process inspired by one of the algorithms for finding Costas arrays for some dimensions, the so-called Welch algorithm (Golomb and Taylor, 1984). In our modification of this algorithm, we first seek the smallest prime  $P$  greater than  $N$ , where  $N$  denotes the total number of shots in the survey. We then look for the largest prime  $T$  less than  $P$  that generates a complete permutation of the numbers from 1 to  $N$  by the following process. First, we calculate the sequence

$$n_j = T^j \quad \text{mod} \quad P , \quad (12)$$

where  $n_j$  ( $j = 1, \dots, P$ ) form a permutation of the numbers from 1 to  $P$ . In this sequence, we eliminate the elements  $n_j > N$  to arrive at the final array, which we refer to as a quasi-Costas array. If we desire redundancy of shots within the set of groups, we change  $T$  to the largest prime less than  $T$  that allows the

construction and repeat the process. Note that the probability for the array found with this process to be a true Costas array decays with increasing  $N$ .

The thus obtained quasi-Costas array defines the sequence in which the shots are grouped. If we want to build groups of  $K$  shots, each set of  $K$  values of this vector defines a group. Note that this construction process of the permutation vector actually has an advantage over the use of true Costas arrays. Because of the limited number of Costas arrays existing for large  $N$ , the exclusive use of these arrays could lead to repeated groups in the case of shot redundancy.

### A posteriori crosstalk reduction

Since it is impossible to prevent the occurrence of crosstalk when shot groups are migrated, another option is to remove it (or part thereof) after migration. Assuming that the noise is random and zero mean, we can apply existing techniques for removing such noise. In this study, we have tested the application of the nonlocal means (NLM) technique borrowed from image processing (Buadès et al., 2005, 2010; Bonar and Sacchi, 2012) and first applied to a seismic problem by Bonar and Sacchi (2012).

The NLM algorithm is a random-noise attenuation filter supposing that every image has a certain degree of redundancy, which can be used to highlight structures. The process searches, for each image point, other points whose neighborhoods are similar to the neighborhood of the original point, and uses these similarities to recover the image in this region. The fundamental process of the algorithm is an average over the whole image, applied with a weight that is determined by the similarities between the image in the vicinities under consideration.

Mathematically, the filtered image  $J$  is calculated from the original image  $I$  by the weighted average

$$J(\mathbf{x}) = \sum_{\mathbf{x}'} \mathcal{W}(\mathbf{x}, \mathbf{x}') I(\mathbf{x}') , \quad (13)$$

where  $\mathcal{W}(\mathbf{x}, \mathbf{x}')$  denotes the filter weights, calculated as

$$\mathcal{W}(\mathbf{x}, \mathbf{x}') = \frac{1}{Z(\mathbf{x})} \exp \left\{ \frac{-D^2(\mathbf{x}, \mathbf{x}')}{h^2} \right\} . \quad (14)$$

Here,  $h$  is a parameter that controls the exponential decrease and  $Z(\mathbf{x})$  is a normalization factor, i.e.,

$$Z(\mathbf{x}) = \sum_{\mathbf{x}'} \exp \left\{ \frac{-D^2(\mathbf{x}, \mathbf{x}')}{h^2} \right\} . \quad (15)$$

Function  $D(\mathbf{x}, \mathbf{x}')$  represents the similarity measure between the vicinities of image points  $\mathbf{x}$  and  $\mathbf{x}'$ . It is calculated as

$$D^2(\mathbf{x}, \mathbf{x}') = \sum_{\mathbf{d}} G_a(d) [I(\mathbf{x} + \mathbf{d}) - I(\mathbf{x}' + \mathbf{d})]^2 , \quad (16)$$

where  $\mathbf{d}$  represents a dislocation vector of size  $d$  and function  $G_a(d) = \exp(-d^2/a^2)$  denotes a Gaussian window taper, in which the parameter  $a$  defines the effective size of the neighborhood.

## NUMERICAL RESULTS

The large number of variables involved, which implies a high amount of comparative tests, makes actual migrations with all possible weights prohibitively expensive. Therefore, to estimate the reduction in crosstalk in the migrated image achieved by the weights (8) to (11), we evaluate the matrices  $\mathbf{W}$  generated by the product (6) of the weights and their proximity to the identity matrix.

An important number in this sense is the ratio between the accumulated energy in the off-diagonal and diagonal elements of matrix  $\mathbf{W}$ ,

$$E = \frac{\sum_{i \neq j} |W_{ij}|^2}{\sum_{i=j} |W_{ij}|^2} \quad (17)$$

for simplicity from now on referred to as “energy factor”. The lower this number, the better  $\mathbf{W}$  approximates the Kronecker delta. Note that for a group of  $K$  shots without encoding, the energy factor always takes the value  $K - 1$ .

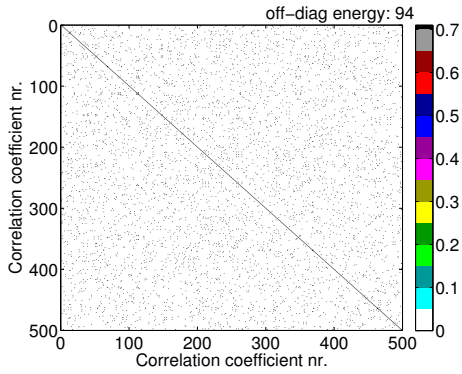


**Figure 1:** No shot encoding, no redundancy, 50 groups of 95 shots (reference matrix).

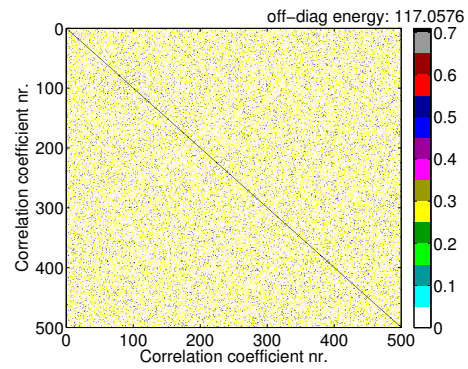


**Figure 2:** No shot encoding, redundancy with 50 groups of 380 shots.

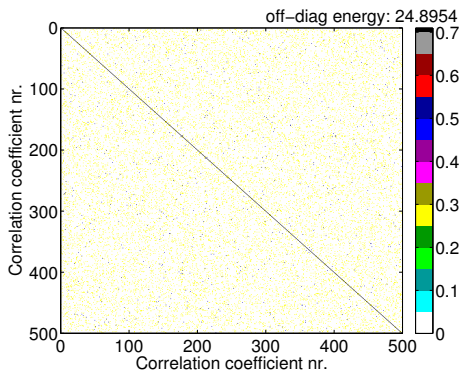


**Figure 3:** No shot encoding, redundancy with 200 groups of 95 shots.

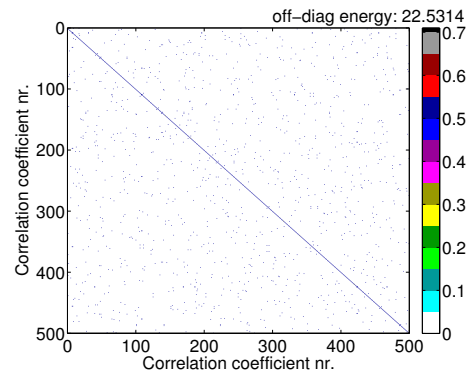


**Figure 4:** No shot encoding, no redundancy, 200 groups of 24 shots.

For all our tests, we have used dimensions of the narrow azimuth data from the EAGE/SEG salt model, i.e., a total of 4750 shots. We have tested various groupings of these shots. If not mentioned otherwise, the comparisons are done with 50 groups of 95 shots each, i.e., no redundancy of shots. The number in the upper left corner of each figure is the energy factor as defined above.

**No encoding.** Figure 1 shows the matrix  $\mathbf{W}$  without shot encoding, i.e., for unit weights,  $w_{gk} = \tilde{w}_{gk} = 1$ . The choice of used sources was made randomly. We note that in this case the off-diagonal energy is 94 times greater than the diagonal energy, corresponding to 95 shots per group, as expected. When increasing the number of shots per group by a factor of four, to 380, the energy factor increases to 117 (Figure 2). Also, when maintaining 95 shots per group and increasing the number of groups to 200, to achieve the same fourfold redundancy, the energy factor reduced to approximately 25 (Figure 3). However, with 24 shots in each of the 200 groups, the energy factor decreased more strongly, to about 22 (Figure 4). We conclude that for a given number of groups, one should use a minimum of sources per group. The use of shot redundancy is counterproductive.

**Random phase encoding.** The next set of figures shows the weight matrices for random phase encoding, for some possible levels of phase shift according to equation (8), for the case of 50 groups of 95 shots. In Figure 5, we see the result of continuous phase encoding, i.e., allowing for all values between  $-\pi$  and  $\pi$ . Figures 6, 7, and 8 show the corresponding results for 16, 10, and 4 levels, respectively. We observe that the continuous distribution yields the strongest reduction of the energy factor.

**Random amplitude encoding.** Figures 9, 10, 11 and 12 show the corresponding results for random amplitude encoding, with continuous distribution and 16, 10 and 4 levels. Again, we observe an increase in energy factor for a decreasing number of levels. In addition, we note that the magnitude of the diagonal is reduced (colored dots on the diagonal, where black indicates a unitary value). This reduction is due to the fact that the product of the weights is not unitary, as mentioned in the context of equation (9).

The fact that the energy factors decreases for a growing number of levels, both for random phase and

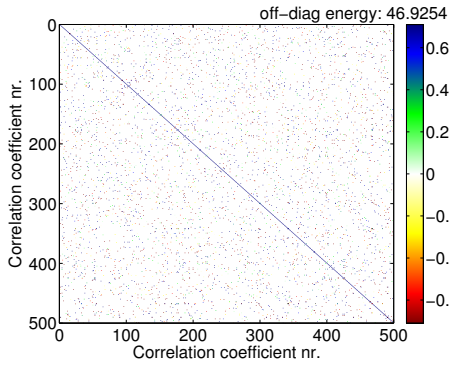


Figure 5: Continuous random phase encoding.

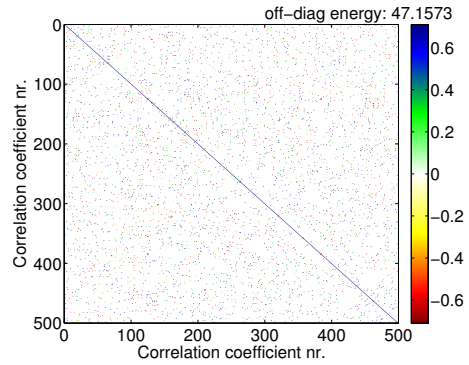


Figure 6: Random phase encoding, 16 levels.

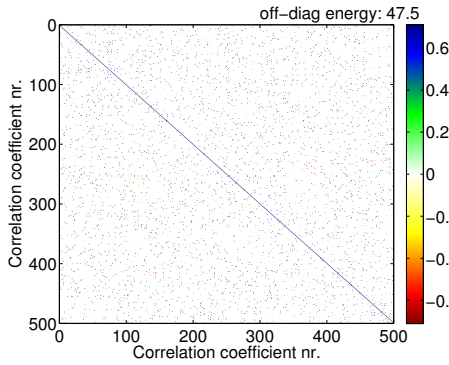


Figure 7: Random phase encoding, 10 levels.

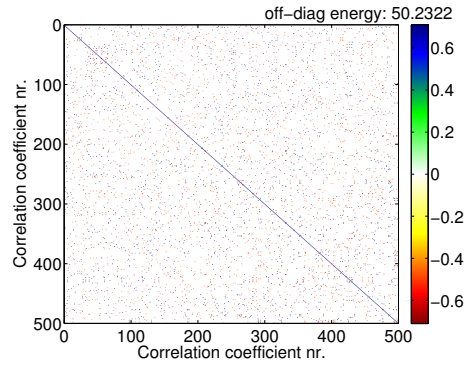


Figure 8: Random phase encoding, 4 levels.

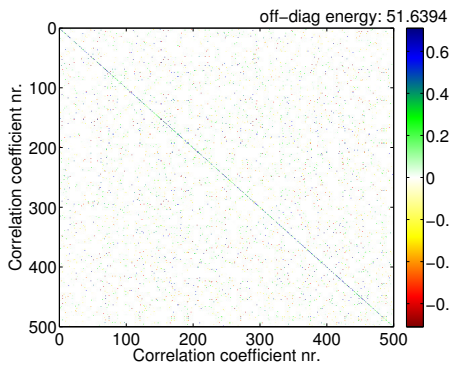


Figure 9: Continuous random amplitude encoding.

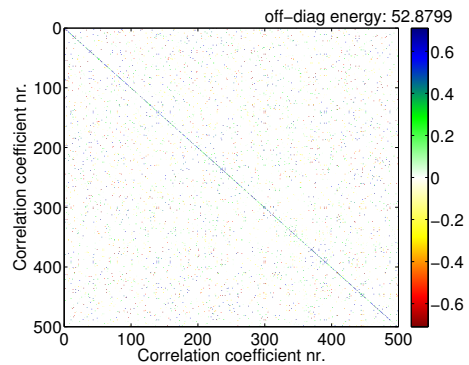


Figure 10: Random amplitude encoding, 16 levels.

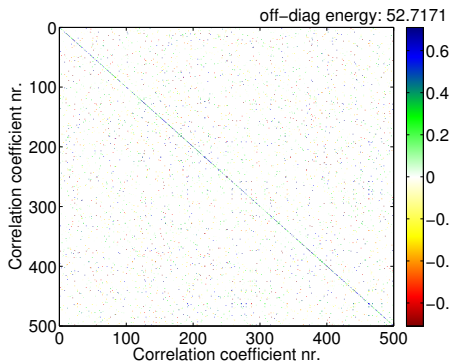


Figure 11: Random amplitude encoding, 10 levels.

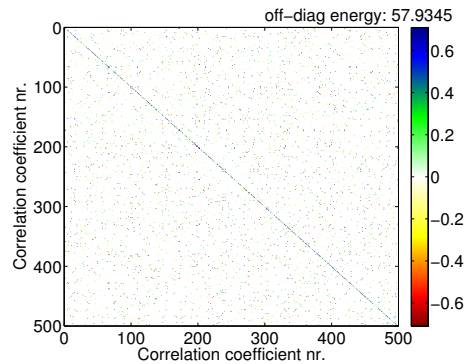
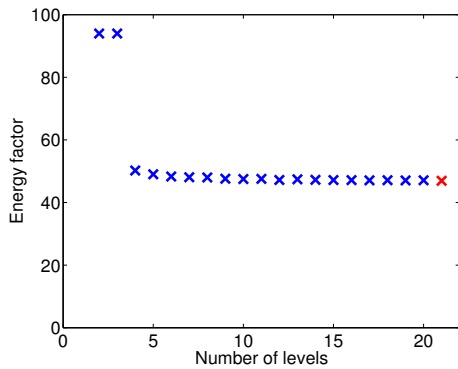
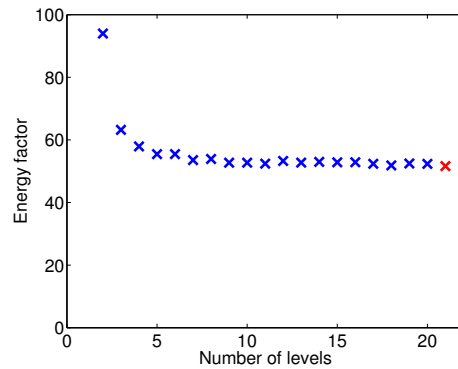


Figure 12: Random amplitude encoding, 4 levels.

amplitude encoding, is corroborated in Figures 13 and 14, which show the energy factor as a function of the number of levels. We see that in both cases, the factor decays with increasing number of levels. We tested



**Figure 13:** Energy factor as a function of level number for random phase encoding.



**Figure 14:** Energy factor as a function of level number for random amplitude encoding.

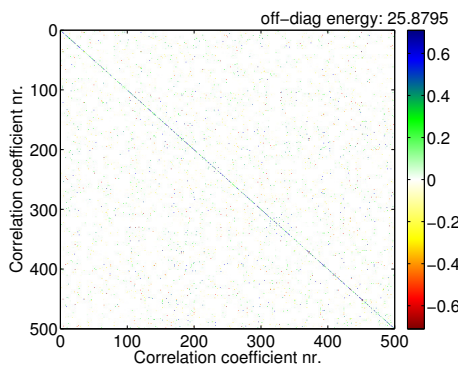


**Figure 15:** Continuous random phase and amplitude encoding.

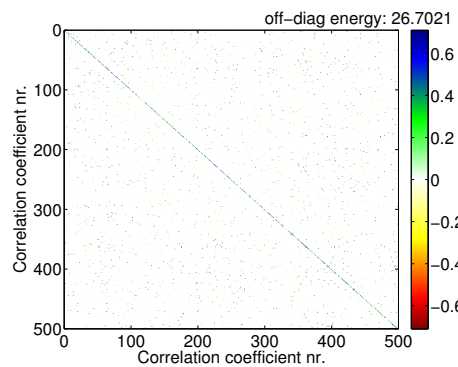


**Figure 16:** Random phase and amplitude encoding, 16 levels.

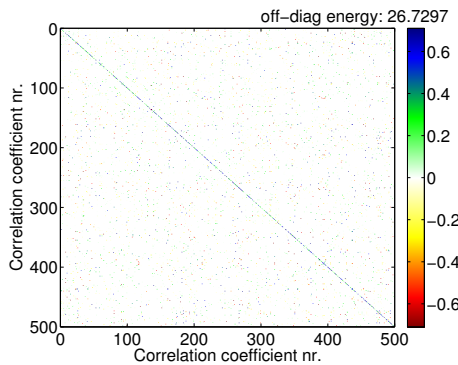


**Figure 17:** Random phase and amplitude encoding, 10 levels.

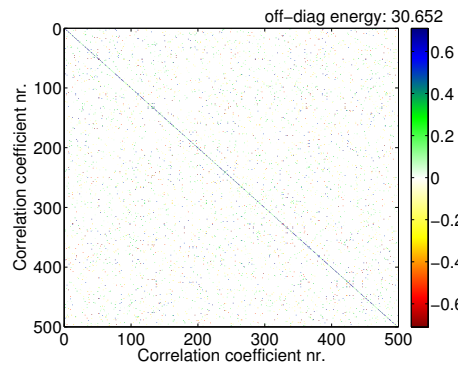


**Figure 18:** Random phase and amplitude encoding, 4 levels.

up to a maximum of 20 levels. The red dot at the end of the curve represents the continuous distribution.

**Random phase and amplitude encoding.** When we apply random encoding of both amplitude and phase, we obtain the matrices shown in Figures 15, 16, 17, and 18. We note that the simultaneous encoding further reduces the power factor, while the diagonal values are comparable with those for random amplitude encoding only. The decay of the energy factor with the number of levels is comparable to previous cases.

To avoid loss of information due to the reduction of the diagonal values, we also tested the effect of redundancy for this type of encoding. Figure 19 shows the weight matrix for 50 groups of 380 shots and Figure 20 shows the weight matrix for 200 groups of 95 shots. We observe the same effect as in the case without encoding, i.e., the energy factor increases with respect to the same number of groups without redundancy.

**Random-sign and imaginary-unit encoding.** Figure 21 shows the result of random sign encoding, equa-

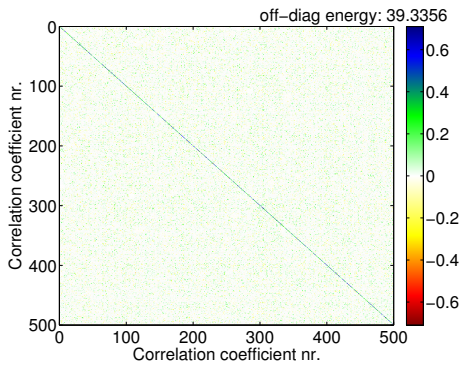


**Figure 19:** Continuous random phase and amplitude encoding, 50 groups of 380 shots.

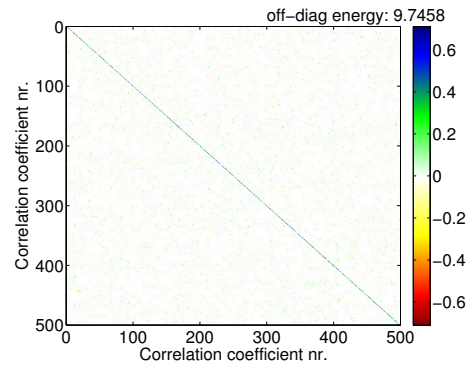


**Figure 20:** Continuous random phase and amplitude encoding, 200 groups of 95 shots.

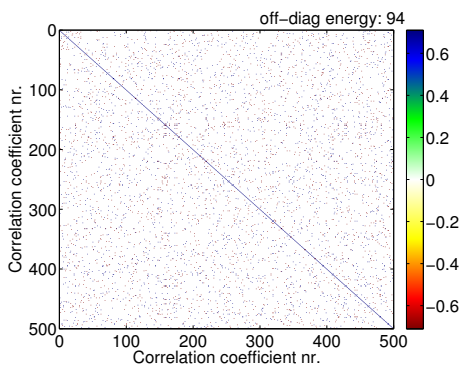


**Figure 21:** Random-sign encoding.

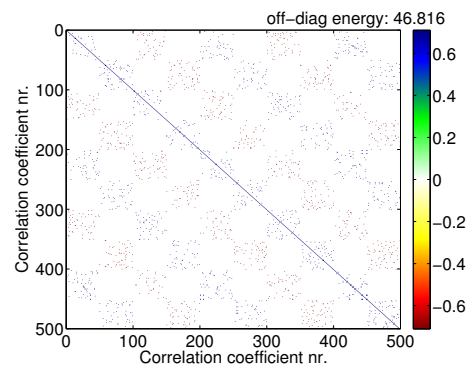


**Figure 22:** Imaginary-unit encoding.

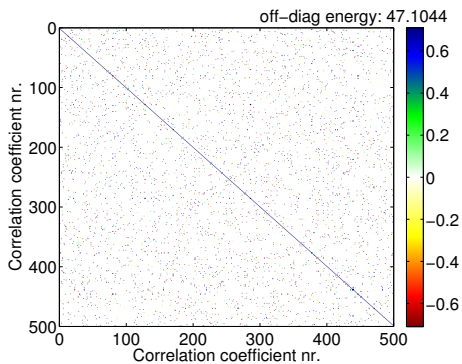


**Figure 23:** Random phase encoding combined with imaginary-unit weighting.

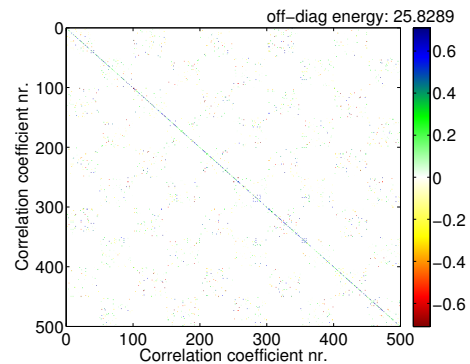


**Figure 24:** Random amplitude encoding combined with imaginary-unit weighting.

tion (10), which is equivalent to random amplitude (or phase) encoding with two levels. We note that this encoding does not reduce the energy factor. Encoding with the imaginary unit, according to equation (11), reduces this factor by half (Figure 22) by transferring half the crosstalk to the imaginary part of the image, which will be discarded.

**Combinations.** Finally, we investigate the combination of the latter weight with random signal, amplitude and/or phase encoding. We note that the combination of random phase encoding with imaginary-unit weighting does not contribute to a further reduction of the energy factor (Figure 23). The reason is that random phase encoding already transfers energy to the imaginary part of the image, thus not offering the potential for a further reduction. On the other hand, the combination of random amplitude encoding with imaginary-unit weighting further reduces the energy factor significantly (Figure 24), reaching the same level as simultaneous random amplitude and phase encoding. The combination of random phase and amplitude encoding with imaginary-unit weighting does not contribute to a further reduction of the energy factor (Figure 25). Finally, the combination of random sign encoding with imaginary-unit weighting only

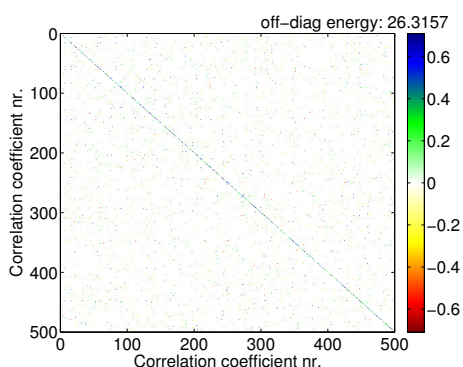


**Figure 25:** Random phase and amplitude encoding combined with imaginary-unit weighting.

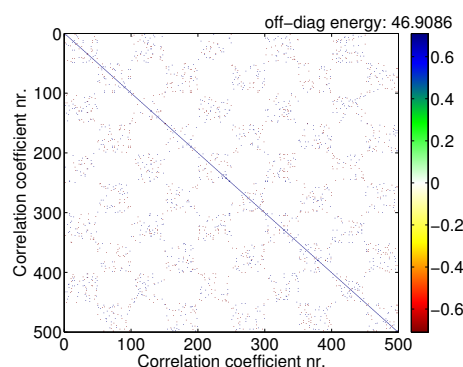


**Figure 26:** Random sign encoding combined with imaginary-unit weighting.

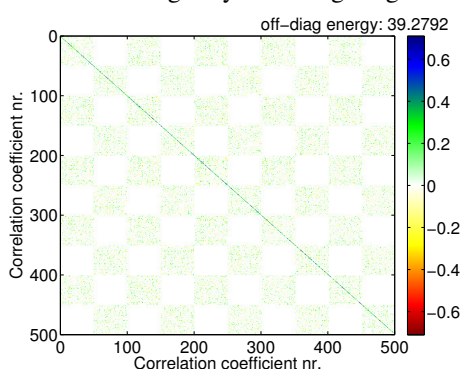


**Figure 27:** Random amplitude encoding combined with imaginary-unit weighting, 50 groups of 380 shots.

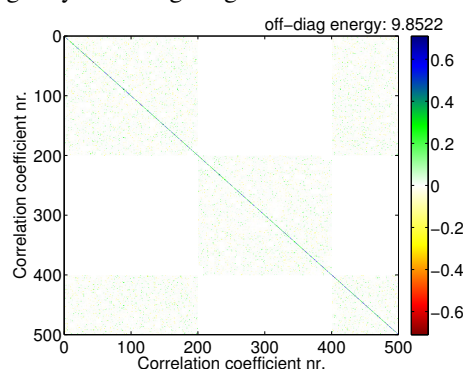


**Figure 28:** Random amplitude encoding combined with imaginary-unit weighting, 200 groups of 95 shots.

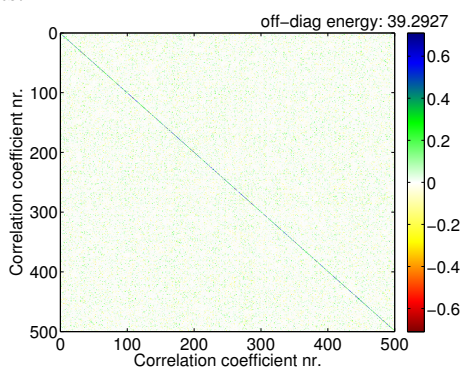


**Figure 29:** Random amplitude and phase encoding combined with imaginary-unit weighting, 50 groups of 380 shots.

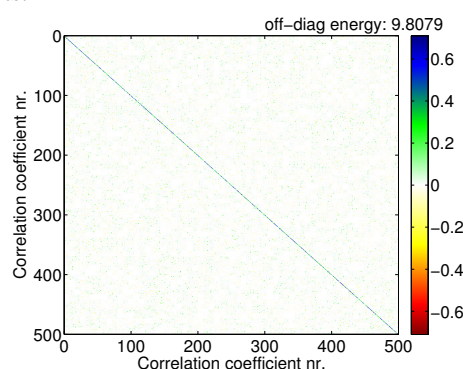


**Figure 30:** Random phase encoding combined with imaginary-unit weighting, 200 groups of 95 shots.

reduces the energy factor to the same level achieved by mere imaginary-unit weighting (Figure 26).

The use of redundancy for random amplitude encoding combined with imaginary-unit weighting (Figures 27 and 28) and random amplitude and phase along combined with imaginary-unit weighting (Figures 29 and 30) leads to the same conclusions as the previous cases.

### 3D migration tests

We implemented a code for 3D finite-difference blended-shot migration with two different choices of shot selection: random and pattern-minimizing. We applied this blended-shot migration to narrow azimuth data from the SEG/EAGE salt model. For simplicity, we tested the shot selection for random phase encoding.

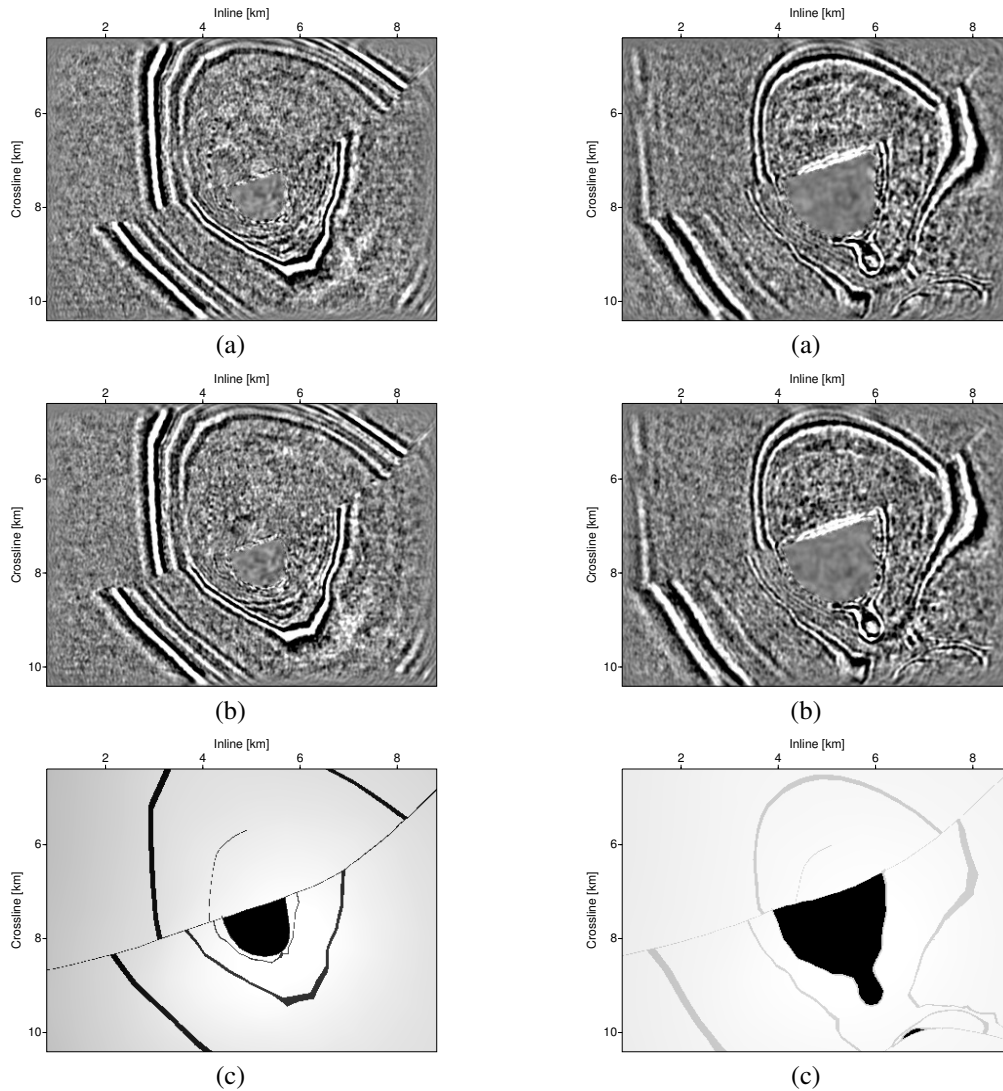


**Figure 31:** 3D FD migrated data from the SEG/EAGE salt model, depth slice at depth 680 m, with (a) random and (b) pattern-minimizing shot selection; (c) model slice.

**Figure 32:** 3D FD migrated data from the SEG/EAGE salt model, depth slice at depth 1040 m, with (a) random and (b) pattern-minimizing shot selection; (c) model slice.

To enhance the effect of crosstalk, migration was performed with a redundancy of 10, using 100 groups with 475 shots.

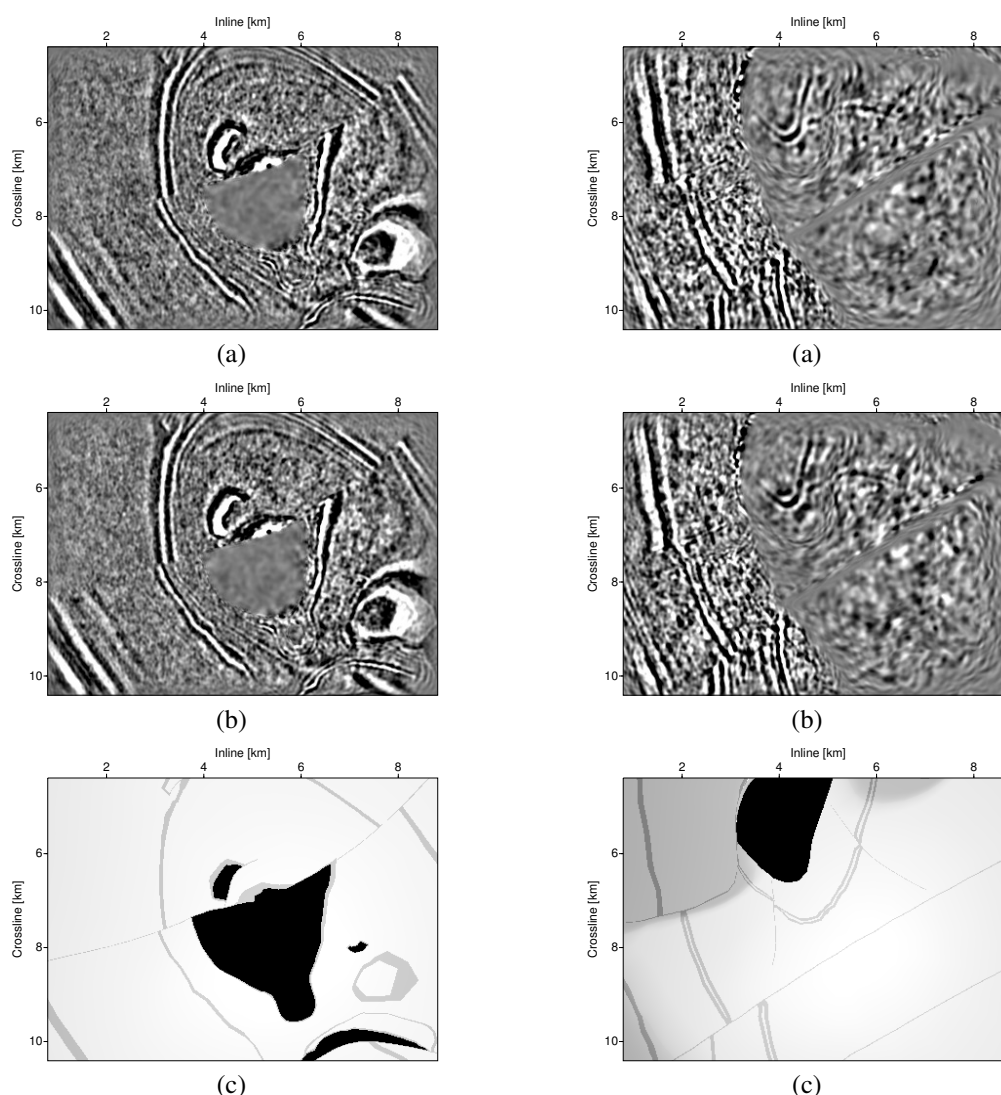
The following figures show depth slices at some selected depths. To our perception, at some depths the slices using pattern-minimizing shot selection are of better quality than those using random shot selection. At all other depths, the quality is comparable. This is the expected behavior, since the pattern minimization is supposed to reduce the probability for correlated shots to appear in the same group.

Figure 31 compares the depth slices at depth 680 m. We observe that the events are clearer in part (b), particularly those close to the salt body in the center of the image.

At 1040 m depth (Figure 32, the differences are more subtle. We can observe a slight improvement in the definition of the right flank of the salt in Figure 32b.

However, not always all properties of the image are better for pattern-minimizing shot selection. While in the salt in Figure 33b is still easier to delineate, particularly in the lower part of the image, the shape of the inclusion on the right side of the image is better represented in Figure 33a.

Since inside the salt, the comparison is diffculted by the effect of the strong velocity contrast in the



**Figure 33:** 3D FD migrated data from the SEG/EAGE salt model, depth slice at depth 1260 m, with (a) random and (b) pattern-minimizing shot selection; (c) model slice.

**Figure 34:** 3D FD migrated data from the SEG/EAGE salt model, depth slice at depth 2340 m, with (a) random and (b) pattern-minimizing shot selection; (c) model slice.

model, our last figure is a slice from below the salt, at depth 2340 m (Figure 34). In this depths, the energy of the events is already significantly reduced by illumination effects. Still, the events in part (b) are generally more continuous and less rugged.

**A posteriori crosstalk reduction.** To reduce crosstalk after blended-shot migration, we have implemented a 2D version of the non-local-means (NLM) algorithm, following the original prescription of Buadès et al. (2005).

Figure 35 compares the result of the NLM method for a depth slice of the image at 1040 m with its original cut. We found that the processing could remove almost all noise caused by cross-talk. However, some less energetic events were also attenuated. As we see in this figure, the result of the reduction of noise depends strongly on the value of parameter  $h$ , equation (14). In our tests, the characteristics of the result did not change as a function of depth. This result demonstrates that it is possible to mitigate crosstalk using image processing methods.

Note that the application of the NLM method consumes a considerable computation time. Thus, a full

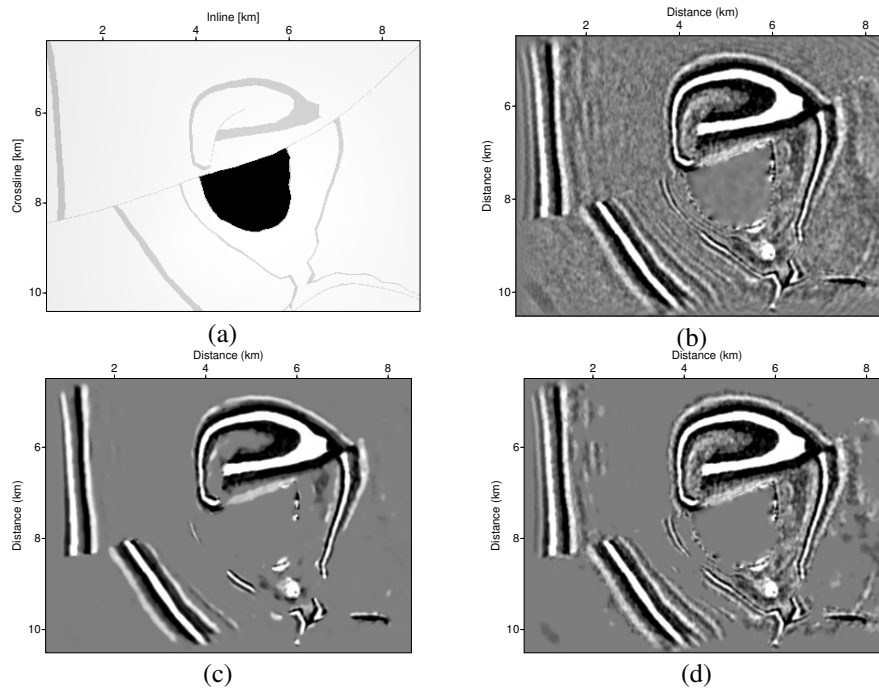


**Figure 35:** Depth slice at 1040 m depth of (a) SEG/EAGE salt model; and of the FD migrated section (b) without noise reduction and with NLM noise reduction with (c)  $h = 10^{-4}$  and (d)  $h = 1.5 \cdot 10^{-4}$ .

3D implementation of this algorithm would be prohibitively expensive. We believe that the implementation can be improved using a modification of the NLM algorithm proposed by Dowson and Salvado (2011) who report significant savings.

## CONCLUSIONS

In this work, we studied the possibilities of reducing the effect of crosstalk in blended-shot migration. In the first part, we evaluated the weight matrix of different encoding techniques.

In these tests, we found that for the investigated encoding methods, there is no advantage in admitting redundancy in the number of shots used. In other words, the choice of the number of shots per group should always be the ratio between the total number of shots acquired and the number of groups to be realized. The fewer shots are contained in each group, the lower is the off-diagonal energy in the weight matrix. This conclusion, however, needs to be confirmed in actual migration tests, since wavefields can show destructive interference, which might help to further reduce crosstalk, even if the content of off-diagonal energy is higher.

Another conclusion from these tests is that random amplitude encoding helps to improve the ratio between the energy on and off the diagonal. Although this encoding reduces the energy contained in diagonal, it reduces the off-diagonal energy more strongly, so that the amplitude of the crosstalk declines more than the amplitude of the image.

Random phase encoding contributes to the reduction of crosstalk mainly by the fact that part of the off-diagonal energy is transferred to the imaginary part of the image. Another way to ensure that this effect is exploited to the maximum is applying a deterministic imaginary-unit weight, which moves every second term of the crosstalk skip to the imaginary part. Thus, the strongest reduction of off-diagonal energy in the weight matrix was achieved by combining this weight with random amplitude encoding. In our examples, this combination reduced crosstalk to approximately a quarter of its nominal value.

In addition to this evaluation of the encoding weights, we studied how to select the shots to form groups to be migrated. Comparing random selection with quasi-Costas-array-based selection, designed to minimize patterns, we observed a trend of the latter to provide less coherent events in the crosstalk.

Finally, we investigated the possibility of reducing the noise generated by crosstalk in a processing step

applied after migration by means of the non-local-means method. In our tests, the noise behaved favorably to this method, so that it was possible to remove much of the crosstalk. This result demonstrates that it is possible to mitigate the crosstalk noise by image processing methods.

#### ACKNOWLEDGMENTS

This work was kindly supported by the Brazilian research agencies CNPq and FINEP as well as Petrobras and the sponsors of the Wave Inversion Technology (WIT) Consortium.

#### REFERENCES

- Beard, J. K., Russo, J. C., Erickson, K., Monteleone, M., and Wright, M. (2004). Combinatoric collaboration on costas arrays and radar applications. In *IEEE National Radar Conference - Proceedings*, pages 260–265.
- Bonar, D. and Sacchi, M. (2012). Denoising seismic data using the nonlocal means algorithm. *Geophysics*, 77(1):A5–A8.
- Buadès, A., Coll, B., and Morel, J. M. (2005). A review of image denoising algorithms, with a new one. *Multiscale Modeling and Simulation*, 4(2):490–530.
- Buadès, A., Coll, B., and Morel, J. M. (2010). Image denoising methods. a new nonlocal principle. *SIAM Review*, 52(1):113–147.
- Claerbout, J. F. (1971). Toward a unified theory of reflector mapping. *Geophysics*, 36(3):467–481.
- Costas, J. P. (1965). Medium constraints on sonar design and performance. Class1 Report R65EMH33, G.E. Corp.
- Dowson, N. and Salvado, O. (2011). Hashed nonlocal means for rapid image filtering. *IEEE Transactions on Pattern Analysis and Machine Intelligence*, 33(3):485–499.
- Drakakis, K. and Rickard, S. (2010). On the construction of nearly optimal golomb rulers by unwrapping Costas arrays. *Contemp. Engineering Sciences*, 3(7):295–309.
- Godwin, J. and Sava, P. (2010). Blended source imaging by amplitude encoding. In *SEG Exp. Abstracts*, pages 3125–3129.
- Godwin, J. and Sava, P. (2011). A comparison of shot-encoding schemes for wave-equation migration. In *SEG Exp. Abstracts*, pages 32–36.
- Godwin, J. and Sava, P. (2013). A comparison of shot-encoding schemes for wave-equation migration. *Geophysical Prospecting*, pages 391–408.
- Golomb, S. W. and Taylor, H. (1984). Constructions and properties of Costas arrays. *Proceedings of the IEEE*, 72(9):1143–1163.
- Guerra, C. and Biondi, B. (2008). Phase encoding with gold codes for wave-equation migration. *SEP Report*, 136:23–42.
- Romero, L. A., Ghiglia, D. C., Ober, C. C., and Morton, S. A. (2000). Phase encoding of shot records in prestack migration. *Geophysics*, 65(2):426–436.
- Soubaras, R. (2006). Modulated-shot migration. In *SEG Exp. Abstracts*, pages 2430–2434. SEG.
- Sun, P., Zhang, S., and Liu, F. (2002). Prestack migration of areal shot records with phase encoding. In *SEG Exp. Abstracts*, pages 1031–1034. SEG.
- Temme, P. (1984). A comparison of common-midpoint, single-shot, and plane-wave depth migration. *Geophysics*, 49(11):1896–1907.